# Nucleation and Growth of Gold on MgO Thin Films: A Combined STM and Luminescence Study

**H. M. Benia,[†] X. Lin,[†,‡] H.-J. Gao,[‡] N. Nilius,*[,†] and H.-J. Freund[†]**

*Department of Chemical Physics, Fritz-Haber-Institut der Max-Planck-Gesellschaft, D-14195 Berlin, Germany, and Beijing National Laboratory for Condensed Matter Physics, Institute of Physics, Chinese Academy of Sciences, P.O. Box 603, Beijing 100080, China*

*Received: April 5, 2007; In Final Form: May 11, 2007*

Electroluminescence measurements have been performed with a scanning tunneling microscope (STM) to study the growth of Au particles on thin MgO films prepared on Mo(001). With increasing Au coverage, rapid quenching of the characteristic, defect-related MgO emission is observed, while a new peak emerges in the optical spectra that is attributed to Mie plasmon resonances of the Au particles. The fast decline of the MgO signal with metal exposure indicates that Au nucleation preferentially takes place at the optically active centers in the MgO surface. The nucleation sites have been identified in STM measurements as being located along the step edges of the MgO surface. A sputter-deposition of Au results in a significantly slower decline of the MgO optical signal, manifesting the delayed blocking of optically active MgO centers due to Au nucleation on artificial surface defects.

## Introduction

The outstanding catalytic performance of metal particles on oxide supports has been in the focus of research already for many decades.[1] So far, several physical and chemical effects have been identified to be responsible for their unexpected high activity. Consensus is reached on the fact that low-coordinated sites present at the particle surface and a modified electronic structure due to confinement effects within the deposits play a major role for the catalytic activity.[2,3] The chemical properties are also determined by interactions between the metal particles and the oxide support, making only selected metal/oxide combinations suitable for catalytic applications. The substrate influence has been ascribed to several effects, such as (i) control of the nucleation and growth behavior of the metal particles,[4,5] (ii) storing/releasing oxygen during the chemical reaction,[6,7] and (iii) activating the deposits via charge transfer from the oxide support.[8−10] The latter effect involves nucleation of the particles at special oxide sites, e.g., oxygen vacancies, which are able to act as a trap for loosely bound electrons. For example, the unexpected high reactivity of ultrasmall Au particles on MgO in the low-temperature CO combustion has been traced back to a charging of the Au deposits via electron transfer from MgO color centers.[9] The catalytic performance of a metal/oxide system therefore often depends on the spatial correlation between defects and preferential binding sites in the oxide surface, and exact knowledge of the nucleation and growth behavior is essential to understand the chemical properties of the system.

Several techniques are available to investigate the nucleation of metal atoms on an oxide surface. Attachment of adatoms to oxide defects has been concluded from the heterogeneous nucleation behavior observed in temperature- and flux-dependent growth studies on magnesia and alumina.[4,5,11] Other experiments used the alteration of characteristic, defect-induced signals during metal exposure to establish a relationship between nucleation and defect sites in the oxide surface, such as the spin signal from paramagnetic point defects or the infrared-absorption yield of a defect-related adsorption process.[12−14] Also theoretical modeling contributed largely to the understanding of the interplay between defect structure and nucleation behavior of oxide surfaces.[9,10,15−17]

In this paper, we report on a genuine optical approach to investigate the Au nucleation on thin MgO films. The experiments exploit changes in the light emission characteristics of MgO defect sites when exposing the surface to an Au atom flux. The simultaneous appearance of an Au-induced emission line is used to monitor the growth of the metal aggregates. As the luminescence signal is stimulated by electron injection from the tip of a scanning tunneling microscope (STM), this latter technique is available to characterize the local sample morphology after Au deposition.[18] The exploration of the Au nucleation behavior on MgO thin films via two independent channels provides the unique possibility to link optically active oxide sites with those that are responsible for metal nucleation. Comparable information cannot be acquired using conventional surface science approaches.

## Experiment

The measurements are performed in an ultrahigh-vacuum (UHV) STM ($p \sim 5 \times 10^{-10}$ mbar) operated at room temperature.[19] The Beetle-type STM head is surrounded by a parabolic mirror, which enables photon collection from the tip−sample junction. Outside the vacuum chamber, the light is focused onto the entrance slit of a grating spectrograph attached to a liquid-nitrogen cooled CCD detector. The setup allows recording of electroluminescence spectra in a wavelength range between 200 and 1200 nm. The photon emission is stimulated by electron injection form the STM tip into well-defined surface areas imaged before spectral acquisition. The spectra are taken

* Corresponding author. E-mail: nilius@fhi-berlin.mpg.de.
[†] Fritz-Haber-Institut der Max-Planck-Gesellschaft.
[‡] Chinese Academy of Sciences.

10.1021/jp0726891 CCC: $37.00 
Published on Web 06/27/2007

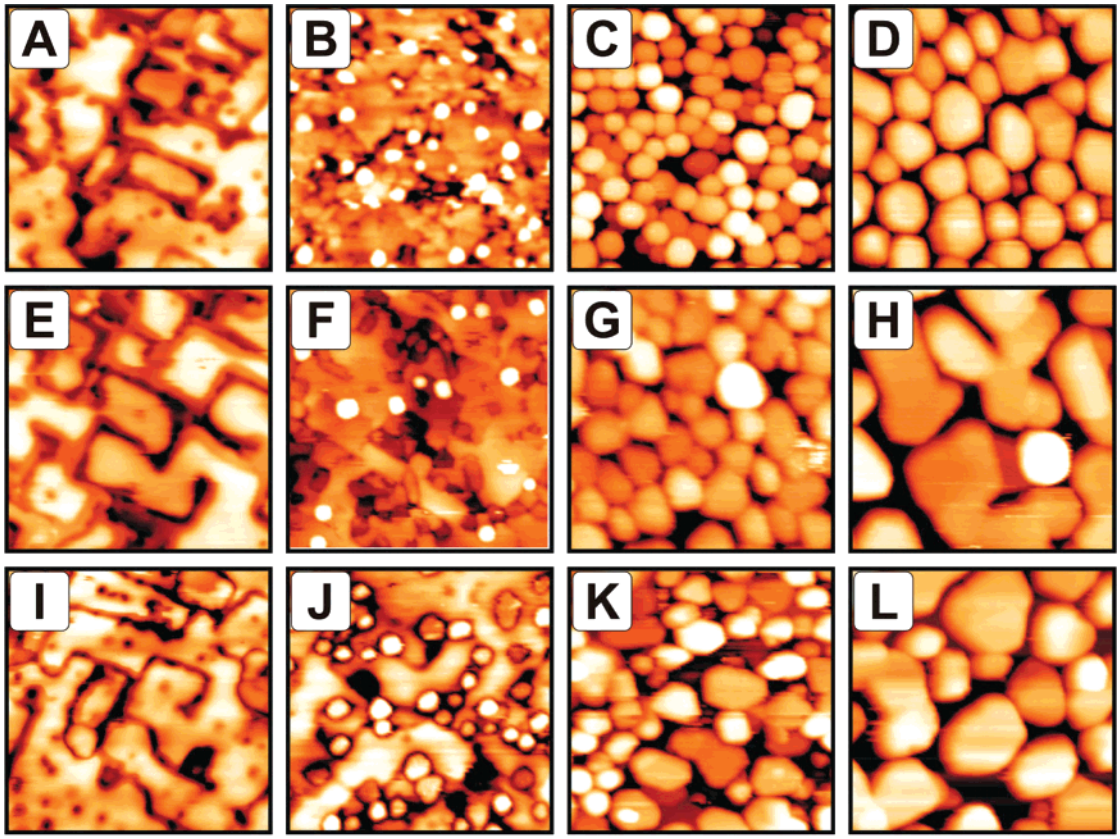


**Figure 1.** STM topographic images of differently thick MgO films grown on Mo(001), before and after deposition of an increasing amount of Au ($50 \times 50$ nm$^2$, $I = 0.05$ nA). Oxide films in A−D and E−H are 7 ML thick (imaging bias: $+3.0\ \text{V} < V_{\text{sample}} < +5.0$ V); films in I−L have a thickness of 14 ML ($+5.0\ \text{V} < V_{\text{sample}} < +8.0$ V). The nominal Au coverage increases from the left to the right in each row, from 0, 0.06, 0.6 to 2.5 ML. While particles in B−D are prepared by a sputter-deposition of Au, those in F−H and J−L are grown in thermodynamic equilibrium.

in the field emission regime of the STM, thereby adjusting the tip−sample distance to approximately 1 $\mu$m and applying a bias of −150 to −200 V to the tip. Electron current and acquisition time per spectra are limited to 1 nA and 60 s, respectively, to minimize the structural damage caused by the impact of high-energy electrons. The spectral information obtained in this way is representative for a surface area of $500 \times 500$ nm$^2$.

The MgO thin films are grown on a Mo(001) single crystal.[20] The Mo surface is cleaned by repeated cycles of $Ar^+$ sputtering, annealing to 1300 K in $O_2$, and flashing to 2300 K in UHV. The procedure results in a sharp $p(1 \times 1)$ low-energy electron diffraction (LEED) pattern and a surface exhibiting large terraces (>200 nm) in the STM. Preparation of the MgO film proceeds via room-temperature deposition of Mg onto the Mo surface in $1 \times 10^{-7}$ mbar $O_2$ and annealing to 1100 K for 10 min to induce crystallization of the amorphous oxide. Surface quality and thickness of the MgO films are monitored by LEED and STM. To explore the influence of the oxide thickness on the Au nucleation behavior, MgO films containing 7 and 14 layers have been used in the experiments. Tunneling through these rather thick MgO films is only possible at elevated positive bias, where electrons are injected into the MgO conduction band and propagate in the tip-induced electric field toward the Mo support.

The Au particles are prepared via vapor deposition from the gas phase onto MgO films held at room temperature. Two deposition schemes are employed, (i) Au evaporation with a negative potential of −800 eV applied between sample and gold doser (referred to as "sputtered sample") and (ii) deposition with doser and sample held at the same potential (referred to as "nonsputtered sample").[21] In the first procedure, a small amount of $Au^+$ ions formed in the evaporation process (<1%) is accelerated toward the MgO surface and creates additional defects, acting as potential Au nucleation sites. In the second case, nucleation takes place exclusively on the preexisting adsorption sites of the oxide film. The coverage is calibrated via Au deposition onto clean NiAl(110), where gold grows in a layer-by-layer fashion and the coverage can directly be determined from STM images. The growth experiments on MgO are performed with Au loads varying between 0.06 and 2.50 monolayers (ML).

**Structural Properties.** A series of STM topographic images, taken for MgO films of 7 ML (top and center) and 14 ML (bottom) thickness and for increasing Au coverage (left to right) is presented in Figure 1. The surface morphology of the clean oxide is characterized by rectangular-shaped islands of 20−50 nm diameter that slightly increase in size with increasing film thickness. The islands are delimited by grooves with ⟨001⟩ orientation, which is the nonpolar step orientation of MgO(001). The morphology reflects typical features of a strained oxide layer, where a network of grooves is introduced to release the 5% lattice mismatch with the Mo support. On the basis of LEED studies, mosaic formation has been identified as an additional means to relax stress and strain in the oxide film.[20,22,23] Details of the structural evolution of MgO films on Mo(001) as a function of thickness are found in a separate paper.[20]

Already small amounts of Au deposited onto the MgO surface (0.06 ML) lead to the formation of aggregates, as revealed from the STM images shown in Figure 1. The Au nucleation density is rather similar for sputtered (top) and nonsputtered samples (middle and bottom) in this growth stage; however, the particle

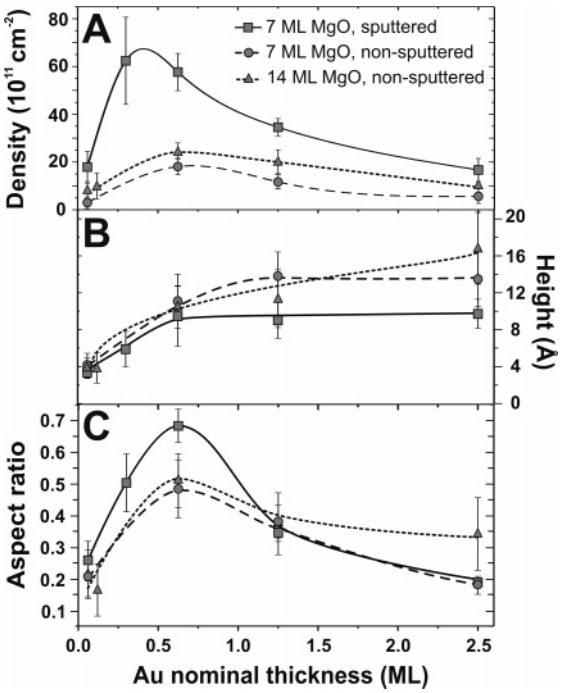


**Figure 2.** Structural parameters of Au particles grown on differently prepared MgO films as derived from STM measurements: **(**A**)** particle density, **(**B**)** averaged particle height, and **(**C**)** height to diameter (aspect) ratio. Triangular and round symbols correspond to a nonsputtered Au deposition onto 14 and 7 ML thick MgO films, respectively. The squares show data for a 7 ML film after sputter-deposition of Au. The lines are guides to the eye.

arrangement distinctively differs for the two preparation procedures. Whereas Au particles are nearly homogeneously distributed for a sputter-deposition with nucleation sites equally located at steps, corners, and terraces, the particles are exclusively found along step edges on the nonsputtered samples. The difference can be attributed to the presence of artificial surface defects on sputtered samples that are created by the impact of energetic $Au^+$ ions during deposition. On nonsputtered samples, heterogeneous nucleation takes place at the low-coordinated step and corner sites that already exist on the oxide surface. The absence of Au particles on extended MgO terraces suggests that point defects are either not available or unimportant for the Au nucleation at room temperature.

In the early growth stage, Au atoms assemble into small, flat islands, indicating enhanced metal−oxide adhesion due to the presence of the Mo support.[24] As a consequence of the larger film thickness, a formation of extended 2D islands as observed for 3 ML MgO on Ag(001) is not detected.[25] With increasing Au coverage (0.5−1.0 ML), the aggregates quickly thicken to compact three-dimensional particles, characterized by aspect ratios (height to diameter) of 0.5 and 0.7 for nonsputtered and sputtered samples, respectively (Figure 2). Following the Wulff construction principle that predicts equilibrium shapes of metal particles on oxide supports, the aspect ratio decreases with increasing adhesion at the metal−oxide interface.[26] The lower aspect ratio observed on nonsputtered samples therefore indicates relatively strong metal−oxide interactions at MgO steps, while the anchoring of particles at artificial defects is comparatively weak. The more striking difference between sputtered and nonsputtered samples is a drastic change in particle density (Figure 2A). For sputtered samples, the density sharply increases with metal exposure and peaks at approximately $65 \times 10^{11}$ particles/cm$^2$. For nonsputtered samples on the other hand, the nucleation density rises only slowly and levels out at a four times smaller maximum value of $15 \times 10^{11}$ cm$^{-2}$.

For even larger amounts of metal precipitated onto MgO/Mo(001) (above 1.0 ML nominal thickness), a third growth regime becomes distinguishable. The initially oblate particles develop into large crystallites with hexagonal or polygonal shapes, indicating the formation of (111) oriented facets. In addition, the particle density starts to decline again as a result of the coalescence between neighboring aggregates on the surface (Figure 2). Coalescence is also responsible for a gradual reduction of the particle's aspect ratios. Due to intergrowth, the lateral particle dimension drastically increases while their height stays approximately constant.

Differences between sputtered and nonsputtered samples are less apparent in the high-coverage regime, as the morphology is not determined by details of the nucleation behavior anymore. However, the particle geometry is still influenced by the MgO film thickness: Particles on thick layers (14 ML) exhibit larger aspect ratios and more 3D-like shapes than those grown on thinner films (7 ML) (Figure 2C). This observation is attributed to a slight increase of the Au−MgO binding strength due to the residual influence of the Mo support, which induces a flattening of the particle shapes according to Wulff's principle.[24] The contribution of the Mo support consists in a transfer of electrons toward the Au deposits, thereby enabling enhanced polarization interactions with the MgO film.[10] With increasing oxide thickness, the Mo contribution vanishes and Au particles take the 3D shapes expected for bulk MgO, as observed in the experiments.

**Optical Properties.** The investigation of the optical characteristics of Au/MgO/Mo(001) provides an independent means to study the nucleation and growth of gold particles on the MgO surface. The approach exploits the alteration of a defect-related MgO photon signal with increasing Au coverage, thus disclosing the interrelation between optical emission sites, defects, and nucleation centers on the oxide film. The luminescence properties of MgO are determined by the radiative decay of coupled electron−hole pairs (excitons), excited via electron or photon injection.[20,27−29] MgO excitons are primarily created at 5-fold coordinated (5C) terrace sites and perform a random-walk type motion across the surface until they become trapped at defects and under-coordinated step (4C) and corner (3C) positions. The trapping occurs as a result of the reduced Madelung potential at sites with lower coordination.[30] A small fraction of excitons decays via radiative recombination and emits photons of well-defined energy, thus providing a fingerprint of the trapping position involved. Exciton recombination at 3C corner and kink sites is commonly connected to the emission of 3.0−3.3 eV photons, while deexcitation at step edges produces photons of 4.0−4.5 eV. The optical characteristics of the MgO surface sites have been predicted by theory and verified experimentally for MgO nanocrystals, smokes, and thin films via photo- and electroluminescence spectroscopy.[20,27−30]

Figure 3 (bottom) presents two photon emission spectra obtained via electron injection into bare MgO films of 7 and 14 ML thickness. The spectra exhibit an asymmetric emission line centered at 415 nm (3.0 eV), which is typical for exciton recombination processes involving 3C corner sites.[20] The intensity at lower wavelength relates to 4-fold coordinated traps, while the origin of the high-wavelength shoulder cannot be specified at the moment. The emission spectra change considerably after gold deposition. Already in the low-coverage regime, the intensity of the 3.0 eV MgO peak dramatically declines, while a new emission line emerges in the wavelength region of

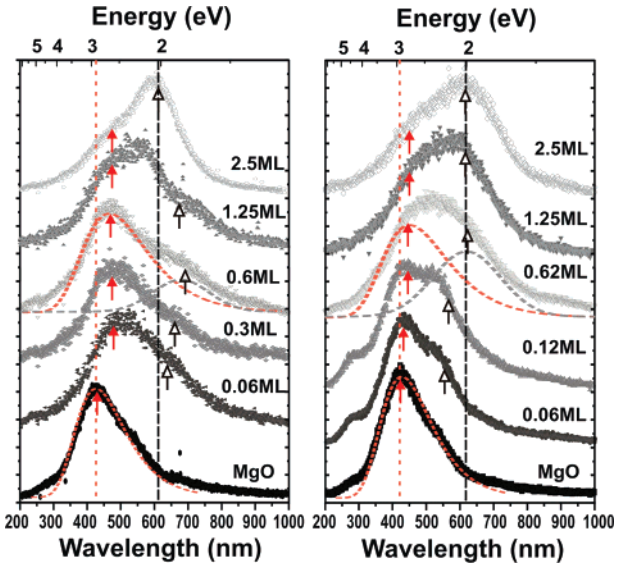


**Figure 3.** Normalized photon emission spectra measured for MgO thin films covered by an increasing amount of Au: **(**A**)** sputter-deposition of Au onto a 7 ML thick MgO film; **(**B**)** nonsputtered Au deposition onto a 14 ML thick film. Spectra are fitted with a symmetric and an asymmetric Gaussian to account for the Au and the MgO contribution within the spectra (as shown for first and fourth spectra from the bottom). Solid and open arrows mark the maximum positions of the MgO and Au fit functions, respectively.

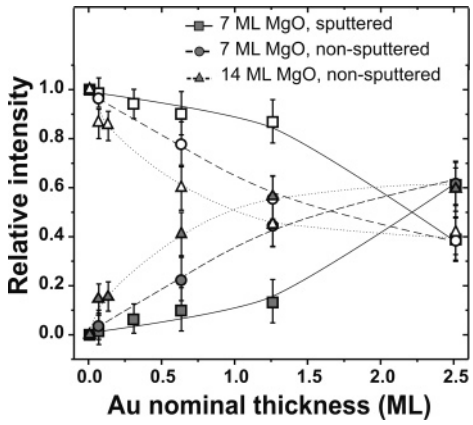


**Figure 4.** Relative contributions of the MgO- and Au-derived photon signals to the integrated emission intensity as a function of Au coverage, derived from spectral series as shown in Figure 3. Triangular and round symbols correspond to a nonsputter deposition of Au onto 14 and 7 ML thick MgO films, respectively. The squares show data for a 7 ML film after sputter-deposition of Au. Closed symbols depict the relative Au intensities; open symbols, the MgO values. The lines are guides to the eye.

550−650 nm (2.2−1.9 eV). With increasing Au exposure, this peak gains intensity with respect to the MgO-related feature and finally dominates the optical spectra for 2.5 ML nominal Au thickness. The new emission line is attributed to the radiative decay of Mie plasmons, excited in the Au particles by the electron injection.[31] Mie plasmons can be viewed as collective electronic excitations in the particle's free-electron gas and determine the absorption and emission characteristics of noble metal clusters due to their extremely high oscillator strength. The plasmon energy is given by the Au dielectric function, the particle shape, and the nature of the dielectric surrounding and can be estimated from calculating the energy-dependent polarizability of a metal sphere in a dielectric medium.[31] Assuming a particle environment composed from 30% MgO ($\epsilon_{MgO} = 3.2$) and 70% vacuum, the plasmon energy computes to 2.2 eV, in reasonable agreement with the peak position in the optical spectra. The assignment of the new emission line to Mie plasmon excitations in Au particles is corroborated by the observation of similar features in the optical response of Au particle ensembles on various dielectric supports.[32−34]

While the general evolution of the luminescence with increasing Au exposure is rather similar for sputtered and nonsputtered samples, a more careful evaluation of the spectra provides valuable insights into the growth characteristics of gold in both cases. The analysis is performed by deconvoluting the emission spectra into intensity stemming from low-coordinated MgO sites and intensity related to Au Mie plasmon resonances. To model the MgO contribution, the photon emission of the bare oxide is described by an asymmetric Gaussian peaking at 415 nm (Figure 3). This spectral shape is kept constant during the following fitting procedure, modifying only the position and intensity of the peak as a function of Au load. A second Gaussian with adjustable height, width, and energy position (confined to a range between 500 and 700 nm) is used to account for the Au spectral contribution. The sum of both components reproduces the experimental spectra and allows a division of the total photon response into an MgO and an Au portion. Absolute emission yields cannot be determined from electroluminescence experiments with an STM, as measured intensities vary between the experimental runs due to changes in the microscopic tip shape and the excitation conditions. Therefore, relative intensities are defined as the ratio between the fitted Au and MgO peak areas ($A_{Au}$, $A_{MgO}$) and the integral intensity: $I_{Au}^{rel} = A_{Au}/(A_{MgO}+A_{Au})$ and $I_{MgO}^{rel} = A_{MgO}/(A_{MgO}+A_{Au})$. This kind of data analysis implicates that relative Au and MgO intensities behave in a mirrorlike fashion and carry the same information.

The evolution of relative intensities with increasing Au coverage can now be used to analyze the quenching of the MgO emission due to Au particles blocking the active sites (Figure 4). The same general trend is found for sputtered and nonsputtered samples as well as for thin and thick MgO films. The MgO-related signal drops from 1.0 (corresponding to bare oxide) more or less rapidly to ∼0.4 for a surface covered with Au particles. The nonzero MgO signal even at high coverage indicates that a fraction of optically active centers survives between the particles. The quenching rate of the MgO signal is, however, rather different for the various preparation procedures. The fastest decay is observed for thick MgO films and a nonsputter deposition of gold, where the intensity decreases roughly exponentially with Au coverage (Figure 4, dotted line). For thin films and sputtered samples, the intensity declines more gradually and follows a roughly linear dependence on the Au load (dashed and solid lines).

This difference is easily understood on a qualitative base: For Au deposition in thermodynamic equilibrium (nonsputtered sample), the particles nucleate at intrinsic MgO binding sites (heterogeneous nucleation). These nucleation sites are apparently identical to the optically active centers in the oxide surface, as manifested by the rapid decay of the MgO emission intensity during Au deposition. Edge, corner, and kink sites have been identified as the characteristic MgO emission centers before; consequently these low-coordinated sites seem to play a decisive role in the Au nucleation process, too. The identity between Au nucleation sites and low-coordinated sites of the MgO surface is corroborated by the STM measurements.

For decreasing oxide thickness, the Au nucleation characteristic is altered by the influence of the Mo support and the

resulting increase of the Au−MgO adhesion. As a consequence, the nucleation process is not exclusively governed by low-coordinated sites anymore but also takes place at MgO terraces.[24] Since 5-fold coordinated terrace sites are not relevant for the emission properties of MgO, the optical response declines less rapidly with increasing Au load. This trend is further amplified for a sputter-deposition of Au onto the MgO films. The impact of high-energy $Au^+$ ions creates new binding sites in the oxide surface, which compete with the intrinsic nucleation centers and diminish their importance in the particle formation process. Consequently, low-coordinated MgO sites remain empty even for higher Au loads and continue to contribute to the optical signal, thus leading to the slower decline of the MgO emission signal observed for sputtered samples.

The general suppression of the MgO photon signal for increasing Au load might be related to (i) an opening of nonradiative decay channels for excitons involving the Au particles or (ii) a reduced trapping probability for excitons at low-coordinated MgO sites capped by Au. The second possibility seems to be less likely, as a new, blue-shifted emission line should appear in the spectra that results from exciton decays at higher-coordinated MgO sites, in disagreement with the experimental results. Exciton decays involving excitation in the Au particles is the more plausible process and could even explain the relatively strong Mie plasmon emission detected from rather small particles. In this scenario, an energy transfer from excitonic modes trapped at the particle's binding site could enhance the excitation cross-section of the Mie plasmon. A possible influence of Au deposits already in the creation process of excitons is excluded here, because MgO terrace sites governing the exciton formation are only sparsely covered with particles at low coverage.

The fitting procedure of the optical spectra also provides information on the position of MgO and Au related emission lines. For the MgO emission line, a red shift is revealed from 415 nm for bare MgO to 455 nm for films covered with 2.5 ML of Au. The shift indicates changes in the dielectric environment and the local electronic structure of the MgO emission centers during Au exposure, thus providing further evidence for a strong interaction between the optically active MgO sites and the Au deposits. Also, the Mie plasmon (here the 1,0-mode) varies considerably in position, which is mainly attributed to changes in the Au particle shape during growth. For nonsputtered samples, the plasmon shifts to lower energies with increasing coverage (2.1 eV → 2.0 eV). This is compatible with the initially increasing and then relatively constant height to diameter ratio, as deduced from the STM images (Figure 2C). For sputtered samples, the Mie energy runs through a minimum at approximately 0.6 ML Au thickness (2.0 eV → 1.8 eV → 2.0 eV), which is related to the formation of particles with large aspect ratios (∼0.7) in this stage. In general, emission lines related to Au plasmon modes are strongly broadened due to the size and shape distribution of particles on the surface.

The picture of the Au nucleation behavior on MgO arising from the present experiments is in general agreement with earlier experimental and theoretical studies. Heterogeneous nucleation was observed for various metals on the MgO surface, indicating the dominant influence of oxide defects in the initial adsorption process.[11,35] For thin MgO films on Ag(001), the defect-assisted nucleation of Au was directly derived from the quenching of the paramagnetic $F^+$ defect signal of MgO with increasing Au load.[36] The importance of oxygen vacancies and low-coordinated edge and corner sites for the adsorption of metal atoms has also been predicted by theory and traced back to a dramatic increase of metal−oxide interactions at surface defects.[9,10,15−17]

## Conclusion

Two independent techniques have been employed to study the nucleation behavior of Au on MgO films grown on Mo(001). From STM measurements, the preferential nucleation sites are identified as the low-coordinated sites located along the oxide step edges. Only for a sputter-deposition of Au, a relevant fraction of particles resides on the MgO terraces. This finding is corroborated by optical measurements, which analyze the quenching of the MgO photon signal stemming from exciton decays at 3-fold coordinated sites. The MgO emission intensity is found to rapidly decrease with Au exposure, indicating a blocking of the optically active centers during the nucleation process. This behavior suggests a spatial proximity or even identity of the intrinsic emission centers and the Au nucleation sites on the MgO surface.

**Acknowledgment.** Support by the European community through STREP GSOMEN is acknowledged.

## References and Notes

(1) *Handbook of Heterogeneous Catalysis*; Ertl, G., Knözinger, H., Weitkamp, J., Eds.; Wiley: Weinheim, Germany, 1997.
(2) Frank, M.; Andersson, S.; Libuda, J.; Stempel, S.; Sandell, A.; Brena, B.; Giertz, A.; Brühwiler, P. A.; Bäumer, M.; Mårtensson, N.; Freund, H.-J. *Chem. Phys. Lett.* **1997**, *279*, 92.
(3) Valden, M.; Lai, X.; Goodman, D. W. *Science* **1998**, *281*, 1647.
(4) Bäumer, M.; Freund, H.-J. *Progr. Surf. Sci.* **1999**, *61*, 127.
(5) Street, S. C.; Xu, C.; Goodman, D. W. *Annu. Rev. Phys. Chem.* **1997**, *48*, 43.
(6) Trovarelli, A. *Catal. Rev.−Sci. Eng.* **1996**, *38*, 439.
(7) Khodakov, A.; Olthof, B.; Bell, A. T.; Iglesia, E. *J. Catal.* **1999**, *181*, 205.
(8) Abbet, S.; Riedo, E.; Brune, H.; Heiz, U.; Ferrari, A.; Giordano, L.; Pacchioni, G. *J. Am. Chem. Soc.* **2001**, *123*, 6172.
(9) Yoon, B.; Häkkinen, H.; Landman, U.; Wörz, A. S.; Antoinietti, J.-M.; Abbet, S.; Judai, K.; Heiz, U. *Science* **2005,** *307*, 403.
(10) Pacchioni, G.; Giordano, L.; Baistrocchi, M. *Phys. Rev. Lett.* **2005**, *94*, 226104.
(11) Haas, G.; Menck, A.; Brune, H.; Barth, J. V.; Venables, J. A.; Kern, K. *Phys. Rev. B* **2000**, *61*, 11105.
(12) Yulikov, M.; Sterrer, M.; Heyde, M.; Rust, H.-P.; Risse, T.; Freund, H.-J.; Pacchioni, G.; Scagnelli, A. *Phys. Rev. Lett.* **2006**, *96*, 146804.
(13) Schauermann, S.; Johanek, V.; Laurin, M.; Libuda, J.; Freund, H.-J. *Chem. Phys. Lett.* **2003**, *381*, 298. Abu Haija M, M.; Guimond, S.; Uhl, A.; Kuhlenbeck, H.; Freund, H.-J. *Surf. Sci.* **2006**, *600*, 1040.
(14) Hollins, P. *Surf. Sci. Rep.* **1992**, *16*, 51.
(15) Yudanov, I.; Pacchioni, G.; Neyman, K.; Rosch, N. *J. Phys. Chem. B* **1997**, *101*, 2786.
(16) Giordano, L.; Di Valentin, C.; Pacchioni, G.; Goniakowski, J. *Chem. Phys.* **2005**, *309*, 41.
(17) Del Vitto, A.; Pacchioni, G.; Delbecq, F. O.; Sautet, P. *J. Phys. Chem. B* **2005**, *109*, 8040.
(18) Nilius, N.; Ernst, N.; Freund, H.-J. *Phys. Rev. Lett.* **2000**, *84*, 3994.
(19) Nilius, N.; Cörper, A.; Bozdech, G.; Ernst, N.; Freund, H.-J. *Prog. Surf. Sci.* **2001**, *67*, 99.
(20) Benedetti, S.; Benia, H. M.; Nilius, N.; Valeri, S.; Freund, H.-J. *Chem. Phys. Lett.* **2006**, *430*, 330.
(21) Benia, H.-M.; Nilius, N.; Freund, H.-J. *Surf. Sci. Lett.* **2006**, *600*, L128.
(22) Wollschläger, J.; Erdös, D.; Goldbach, H.; Höpken, R.; Schröder, K. M. *Thin Solid Films* **2001**, *400*, 1.
(23) Dynna, M.; Vassent, J. L.; Marty, A. *J. Appl. Phys.* **1996**, *80*, 2650.
(24) Ricci, D.; Bongiorno, A.; Pacchioni, G.; Landman, U. *Phys. Rev. Lett.* **2006**, *97*, 036106.
(25) Sterrer, M.; Risse, T.; Heyde, M.; Rust, H.-P.; Freund, H.-J. *Phys. Rev. Lett.* **2007**, *98*, 206103.
(26) Wulff, G. *Z. Kristallogr. Mineral.* **1901**, *34*, 449.
(27) Anpo, M.; Yamada, Y.; Kubokawa, Y.; Coluccia, S.; Zecchina, A.; Che, M. *J. Chem. Soc., Faraday Trans. 1* **1988**, *84*, 751.
(28) Hacquart, R.; Krafft, J. M.; Costentin, G.; Jupille, J. *Surf. Sci.* **2005,** *595*, 172.
(29) Stankic, S.; Muller, M.; Diwald, O.; Sterrer, M.; Knözinger, E.; Bernardi, J. *Angew. Chem., Int. Ed.* **2005**, *44*, 4917.

(30) Shluger, A. L.; Sushko, P. V.; Kantorovich, L. N. *Phys. Rev. B* **1999**, *59*, 2417. Sushko, P. V.; Gavartin, J. L.; Shluger, A. L. *J. Phys. Chem. B* **2002**, *106*, 2269.

(31) Kreibig, U.; Vollmer, W. *Optical Properties of Metal Clusters*; Springer Series Materials Science, Vol. 25; Springer: Berlin, 1995.

(32) Schmitt, J.; Mächtle, P.; Eck, D.; Möhwald, H.; Helm, C. A. *Langmuir*. **1999**, *15*, 3256.

(33) Nilius, N.; Ernst, N.; Freund, H.-J. *Surf. Sci.* **2001**, *478*, L327.

(34) Link, S.; El-Sayed, M. *Annu. Rev. Phys. Chem*. **2003**, *54*, 331.

(35) Henry, C. R.; Meunier, M. *Mater. Sci. Eng., A* **1996**, *217*, 239.

(36) Sterrer, M.; Yulikov, M.; Fischbach, E.; Heyde, M.; Rust, H. P.; Pacchioni, G.; Risse, T.; Freund, H.-J. *Angew. Chem., Int. Ed.* **2006**, *45*, 2630.